JOURNAL OF APPLIED ELECTROCHEMISTRY 17 (1987) 370–384

Enhanced mass transfer using roughened rotating cylinder electrodes in turbulent flow

D. R. GABE, P. A. MAKANJUOLA*

Department of Materials Engineering and Design, University of Technology, Loughborough, Leicestershire LE11 3TU, UK

Received 9 December 1985; revised 26 March 1986

Cylindrical electrodes have been roughened by machining groove patterns, pyramidal knurling, and superimposing wires and meshes for which the degree of roughness has been calculated. By rotating the electrodes in a turbulent regime, mass transfer for cathodic copper electrodeposition has been measured and the degree of consequent enhancement (relative to an equivalent smooth cylinder) calculated. Typically, the surface area has been increased by 10–40% and the mass transfer rate by 100–300% for turbulent flow defined by $7000 < Re < 80\,000$.

Nomenclature

A (A_R)	area of cathodic (rough) cylinder (cm^2)
C	exponent
C_B	metal ion concentration in bulk solution ($mol\,cm^{-3}$)
d_s (d_R)	diameter of smooth (rough) cylinders (cm)
D	diffusion coefficient of metal ion ($cm^2\,s^{-1}$)
F	Faraday's constant.
I_L	limiting current density ($mA\,cm^{-2}$)
j_0	dimensionless mass transfer factor ($=ShSc^c$)
k_L	mass transfer coefficient ($=I_L/zFC_B$)
k_s, k_R	k_L values for smooth and rough cylinders
m, n	exponents
P	pitch, or roughness element spacing (cm)
Re	Reynolds number ($=Ud/v$)
Re'	$d_R U_R/v$
Re_s	dU_s/v
Sc	Schmidt number ($=v/D$)
Sh	Sherwood number ($=k_L d/D$)
St	Stanton number ($=k_L/U$)
U_s (U_R)	peripheral velocity at smooth (rough) cylinders ($cm\,s^{-1}$)
U_0	'friction' velocity ($cm\,s^{-1}$)
w	width of wire mesh opening (cm)
z	valency change, number of electrons
ε	groove depth (cm)
v	kinematic viscosity ($cm^2\,s^{-1}$)
χ	groove width

1. Introduction

Increase in mass transport for an electrochemical process can be achieved by modifying either the solution parameters (concentration, diffusion coefficient, viscosity, etc.) or the electrode physical and geometrical parameters (surface area, ratio of area to volume, etc.). A particularly effective method is to roughen the electrode surface to provide increased area and if this is combined with agitation and fluid flow, further enhancement occurs. This technique is well established [1–3] for both mass and heat transfer, but is generally used in an empirical manner because until recently the specific contribution of increased area and increased agitation during electrodeposition have not been adequately separated because the roughness is continuously changing as powder deposits form.

In earlier studies the rotating cylinder electrode (RCE) has been used to explore turbulent mass transfer effects in metal electrodeposition

* *Present address*: Arthur Andersen Co., Lagos, Nigeria.

0021–891X/87 $03.00 + .12

Table 1. Attached wire elements

Electrode symbol	*Base diameter* (d_R) *(cm)*	*Wire diameter (cm)*	*Pitch or width of opening (cm)*	*Estimated total surface area* (A_R) *(cm^2)*	*Roughness factor* (A_R/A_s)
Wire winding					
WR1	3.05	0.005	0.2	63.39	1.068
WR2	3.05	0.01	0.4	63.39	1.068
WR3	3.05	0.0125	0.5	63.39	1.068
Weave screen					
WW1	3.05	0.0132	0.0185	199.85	3.366
WW2	3.05	0.0173	0.0621	136.16	2.293
WW3	3.05	0.0234	0.1036	125.24	2.109

[4, 5], and the effects of roughness have been recognized and exploited in the ECOCELL process [5–8]. Most recently, the effects of surface roughness as a means of enhancing mass transfer have been studied, particularly for dilute solutions where rates of electrodeposition are slowest [9, 10], and by means of artificially roughened electrodes the relative effects of area enlargement and friction have been measured [11].

In this investigation, a wide range of cylinders has been roughened by knurling machining and superimposing wires; their physical characteristics of area and roughness have been defined and the consequent mass transport rates measured and correlated. By comparison with the equivalent smooth electrodes, degrees of enhancement have been calculated and preferred types of roughness recognized.

2. Experimental details

Experiments were conducted using a rotating electrode rig which has been described in detail elsewhere [9]. The vertical rotating shaft was driven by a stabilized d.c. motor and was controlled to within 1.5% of a selected speed which was typically in the range 200–1800 r.p.m. The reference electrode was a mercury–mercurous sulphate (MMS) electrode connected via neoprene tubing to a 1.0 M Na_2SO_4 salt bridge solution, the sulphate ions from the bridge being compatible with the supporting electrolyte of sulphuric acid. The methods employed for the production of artificially roughened electrodes, detailed in Table 1, are described below.

2.1. *Knurling*

The knurling tools exhibited two main characteristic patterns, straight and spiral. The tool holders were of two types; one held three pairs of tools on a revolving head, and with the other type, it was possible to interchange single tools by removing and then replacing a metal pin. The knurling tools which were fitted onto the single-head tool holder produced two-dimensional 90° triangular grooves. On the other hand, a pair of left- and right-hand spiral tools, available on the more robust holder provided a checkered three-dimensional pattern. Each pattern constituted three standard cut-sizes, namely fine (0.635 mm pitch), medium (1.0 mm pitch) and coarse (1.45 mm pitch).

The knurling process adopted has been described previously [11]. At the start, a length of stainless steel cylindrical rod was machined on a lathe to a diameter of 3.0 cm, as represented by smooth electrode S3. By applying discrete amounts of pressure on the tool holder against a smooth cylinder whilst the tool travelled to and fro along its length, troughs subtending 90° angles were created. In this way, sharp-crested longitudinal (PL), spiral (PS) and also pyramid-type (PP) knurled cylinders were obtained. For the special cases of truncated pyramids (electrodes TP1 to TP3), as was the case with truncated 'V' grooves (TL1 to TL6), the knurling

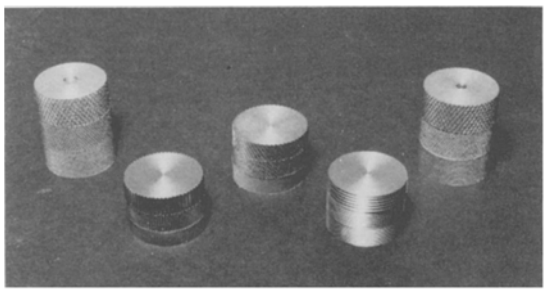

Fig. 1. Photograph of knurled and grooved cylinders.

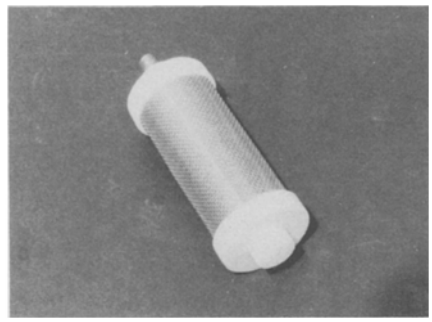

Fig. 2. Photograph of weave-covered cylinders.

process was terminated before the cutting teeth had gone down to the maximum depth.

The maximum external diameter of each of the knurled electrodes was carefully measured using a vernier caliper. When the roughness elements were not perfectly formed, i.e. those with truncated profiles, the roughness height was determined with the aid of a travelling microscope and the average value was calculated.

2.2. *Screw cutting*

In order to produce circumferentially grooved electrodes (PC) a tool-bit was fashioned to provide a 90° blade. The approximate number of grooves per inch corresponding to fine, medium and coarse pitches was determined and by observing the grooves as they were being formed, under a magnifying glass, it was possible to note when sharp crests had been created.

From each of the rough cylinder electrodes machined, a disc sample featuring the roughness pattern was taken from its lower end (Fig. 1) before the standard length of 6.3 cm was fixed. Prior to an experimental run each electrode was fitted with a pair of inert PTFE caps.

2.3. *Weave-covered foil*

A piece of stainless steel, plain weave material was wrapped around a stainless steel cylindrical foil which had been welded beforehand. The new weave seam was superimposed onto the welded joint and the assembly was placed within the welding jig constructed especially for this purpose. Using an electron-beam welding machine, a rough non-integral foil electrode was obtained. This foil was then fitted onto a perfectly matched stainless steel former which was equipped with a pair of PTFE end-caps (see Fig. 2).

2.4. *Wire winding*

It was difficult to establish a method of wrapping stainless steel wire elements longitudinally around cylindrical foils. The first step involved the provision of tiny notches of known pitch at either end of a stainless steel cylindrical foil. Three relatively fine wire sizes (Table 1) provided satisfactorily close wire–foil contact. PTFE tape was wrapped around the foil edges and a tight surface contact was ensured lengthwise with the aid of overlapping PTFE caps.

Area calculations for the rough electrodes were made by the method described in much detail elsewhere [11, 12]. Full electrode specifications are provided in Table 2.

2.5. *Limiting-current measurements*

The electrolyte employed in this study was a 0.014 M $CuSO_4$; 1.5 M H_2SO_4 solution. Details of the experimental technique and procedure have been described [13]; this involved the determination of a 'limiting' overpotential, E_L, which corresponded to limiting current conditions. In the case of smooth cylinders, E_L had a value of -910 ± 10 mV (versus MMS), but for the artificially roughened electrodes considered, a value of -1000 ± 10 mV (versus MMS) was usual. During each run a potential step was applied for a period of 90 s after the desired rotational speed had been set. A current–time plot was obtained on a chart recorder while the overpotential applied to the working electrode

Table 2. Machined roughness elements

Electrode symbol	*Diameter* (d_0) *(cm)*	*Roughness height* (ε) *(cm)*	*Effective diameter* ($d_0 - 2\varepsilon$) *(cm)*	*Roughness pitch* (P) *(cm)*	*Number of roughness elements* (N)	*Effective surface area* (A_R) *(cm^2)*	*Roughness factor* (A_R/A_S)
Longitudinal 'V' grooves[a]							
TL1	3.0	0.0174	2.965	0.1496	63	65.091	1.096
TL2	3.0	0.0262	1.948	0.1496	63	68.029	1.146
TL3	3.0	0.0404	2.919	0.1496	63	72.633	1.223
TL4	3.0	0.0540	2.892	0.1496	63	77.078	1.298
TL5	3.0	0.0216	2.957	0.1024	92	69.668	1.173
TL6	3.0	0.0335	2.933	0.1024	92	75.464	1.271
PL1	3.033	0.03175	2.9695	0.0635	145	82.032	1.381
PL2	3.049	0.05	2.949	0.10	91	81.065	1.365
PL3	3.069	0.0725	2.924	0.145	63	81.365	1.370
Circumferential 'V' grooves[a]							
PC1	3.0	0.03175	2.9365	0.0635	98	81.184	1.367
PC2	3.0	0.0518	2.8964	0.1036	60	79.991	1.347
PC3	3.0	0.0725	2.855	0.145	43	79.062	1.331
Spiral 'V' grooves[a]							
PS1	3.020	0.03175	2.9565	0.0635	124	82.400	1.388
PS2	3.059	0.05	2.958	0.10	78	81.616	1.374
PS3	3.072	0.0725	2.927	0.145	53	80.401	1.354
Pyramidal[a]							
TP1	3.015	0.0231	2.9688	0.0635	~12480	76.445	1.287
TP2	3.035	0.0332	2.9686	0.10	~4970	74.179	1.249
TP3	3.031	0.0498	2.9314	0.145	~2330	74.278	1.251
PP1	3.032	0.03175	2.9685	0.0635	~12480	83.094	1.399
PP2	3.040	0.05	2.940	0.10	~4970	82.890	1.386
PP3	3.067	0.0725	2.922	0.145	~2330	81.775	1.377

[a] Length = 6.30 cm.

was monitored, using a potential pick-up brush situated in its vicinity, on a high-impedance digital voltmeter.

The rotational speed was varied from 200 to 1800 r.p.m. for cylinders of all diameters (see Tables 1 and 2) while the electrolyte composition was maintained constant by employing a concentric soluble copper anode, 8.0 cm in diameter: the cell was thus concentric and undivided. The solution temperature was set at 22 ± 0.2° C.

3. Results

The rate of mass transfer to the surface of a typical rotating cylinder electrode was determined by the evaluation of a mass transfer coefficient, k_L, from the following relation:

$$k_L = \frac{I_L}{AzFC_B} \tag{1}$$

where $k_L = k_R$, given by

$$k_R = \frac{I_L}{A_R zFC_B} \tag{2}$$

for rough RCEs, and employed in the calculation of modified dimensionless numbers, namely either

$$Sh' = \frac{k_R d_R}{D} \tag{3}$$

where d_R represents roughness-root diameter or an equivalent diameter, or

$$St' = \frac{k_R}{U_R} \tag{4}$$

both measured at the corresponding values of modified Reynolds number, namely

$$Re' = \frac{d_R U_R}{\nu} \tag{5}$$

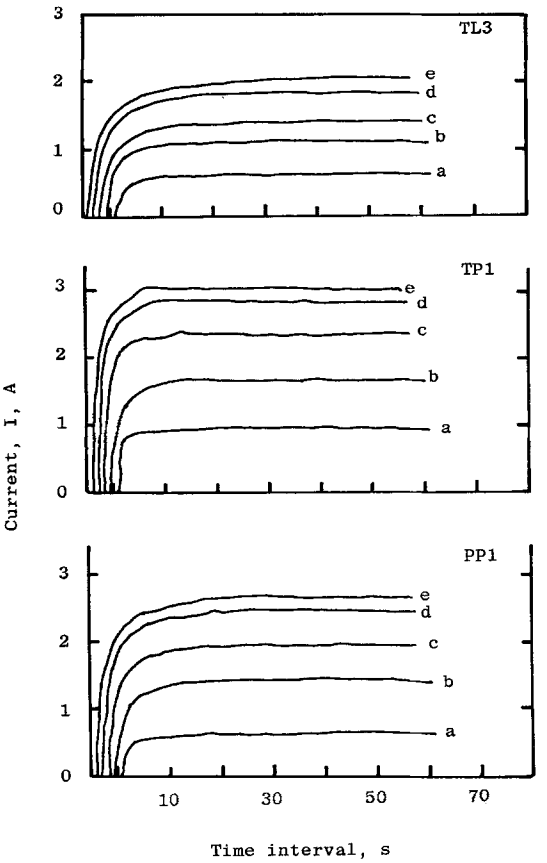

Fig. 3. Relationship of current and time for rough cylinders at −1000 mV (versus MMS) at (a) 200 r.p.m; (b) 500 r.p.m; (c) 800 r.p.m; (d) 1200 r.p.m; (e) 1500 r.p.m. (a) Longitudinal 'V' grooved cylinder TL3; (b) pyramidal knurled cylinder TP1; (c) pyramidal knurled cylinder PP1.

A mass transfer enhancement factor (EF) has been defined as follows,

$$\mathrm{EF} = \frac{St_R}{St_s} = \frac{k_R}{U_R}\frac{U_s}{k_s} \qquad (6)$$

and is evaluated at the corresponding value of $Re_s = U_s d/\nu$, where the smooth electrode dimension, d, represents the projected diameter of a comparable rough electrode. EF denotes the relative mass transfer performance of a rough RCE with respect to an equivalent smooth cylinder.

For the electrolyte composition considered, the diffusion coefficient, D, was evaluated from the expression obtained by Quickenden and Jiang [14]. The value of the kinematic viscosity, ν, was taken from the plot of ν against temperature reported by Robinson [15].

The mass transfer results obtained with smooth electrode S3 have already been published [11]. Such data represented the basis of comparison, at comparable Reynolds numbers, for the array of rough electrodes studied (Tables 1 and 2). From the experiments, sample tracings of I_L against time are shown in Fig. 3a–c. The data for each set of rough electrodes have been plotted as modified Sherwood number (Sh') against modified Reynolds number (Re'). In this way, the Reynolds number index n, as represented in a mass transfer correlation of the form

$$Sh = \text{const}\ Re^n Sc^m \qquad (7)$$

can be determined. At all times Sc was not considered to be a systematic variable and m was assumed constant at 0.356 [13].

A comparison of the performances of the most effective mass transfer enhancers from each group of roughness elements is presented as a plot of St_R/St_s against Re'.

4. Discussion

In this section the mass transfer behaviour of each type of roughness element investigated is discussed under a separate heading. At the close, comparative performances are summarized. The Reynolds number has, typically, been varied between 8000 and 70 000 while the Schmidt number was held constant at 1825.

4.1. *Longitudinally grooved roughness elements*

4.1.1. Effect of roughness height; constant pitch. This study can be considered a direct successor to that reported earlier [11]. TL1 to TL4 were machined to exhibit truncated 'V' grooves with p/ε ratios of 8.33, 5.53, 3.59 and 2.69, respectively. Using a similar coarse-pitched (p = 1.45 mm) knurling tool, electrode PL3 was produced with a p/ε ratio of 2.0 (Table 1) and thus represented the minimum ratio possible for a 90° groove angle. A combined plot of modified Sherwood number versus modified Reynolds number for all five electrodes of this group is shown in Fig. 4. Electrode TL1 provided the lowest mass transfer enhancement, especially for $8000 < Re < 2000$. Presumably, the roughness troughs were so shallow that in this lower

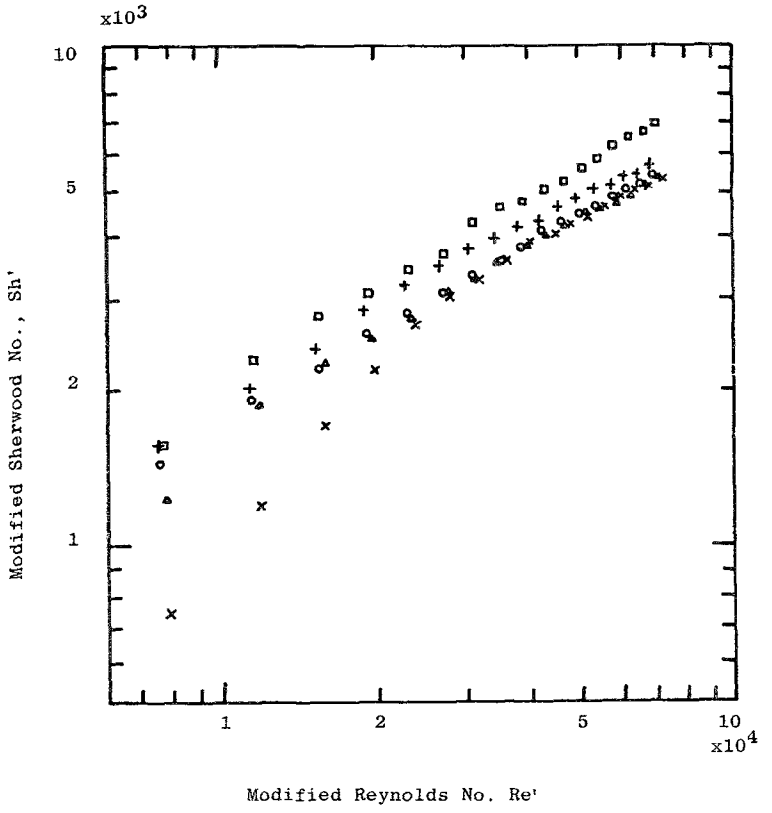

Fig. 4. Mass transfer correlations for longitudinally grooved cylinders TL1 to TL4 and PL3. ×, TL1; △, TL2; ○, TL3; +, TL4; □, PL3.

Reynolds number range an unsteady eddy action was predominant. The apparent similarity in the performances of electrodes TL1 to TL3 for $Re > 20\,000$ may be attributed to sustained eddying within the troughs. In effect, within the bounded walls of a typical longitudinal groove, the scale of motion of surface eddies was probably comparable to the groove depth, ε. In a separate study, which dealt with mass transfer from large rectangular cavities at a planar surface, Jarrett and Sweeney [16] proposed that such behaviour be described as 'captured' vortex or eddies within a cavity during transverse turbulent flow.

During such 'quasi-smooth' boundary flow, as hypothesized above, it may be expected that the magnitude of the mass transfer coefficient ought to be fixed for similar roughness elements on the basis of equivalent surface area. However, electrode TL4 showed an improvement of about 20% above the mean value obtained for electrodes TL1 to TL3 in the high Reynolds number range. A possible explanation for this pattern of behaviour could be the relative closeness of adjacent grooves, i.e. the width of a crest, which might have encouraged the beginning of wake-interference between formerly independent enclaves [17]. For $Re > 20\,000$, electrode PL3 provided an enhancement factor ranging from 2.6 to 2.44; electrode PL3 may thus appear to have exhibited maximum benefit from 'wake-interference' whereas, for truncated grooves, most of the wake effect seems to have been dissipated in the free stream. Similar deductions could be advocated for the relative performance of electrode PL2 in relation to another pair of electrodes, i.e. TL5 and TL6, each of which possessed a similar pitch dimension.

The foregoing interpretation can be extended to describe the relative performances of electrodes TL3 and TL5 for which the roughness pitch measurements were 0.149 and 0.1 mm, respectively. Although electrode TL3 had the greater groove depth, it was still outperformed by the latter by up to 15%. This illustration will tend to emphasize the significance of crest width with regard to possible wake-interference between adjacent groove elements.

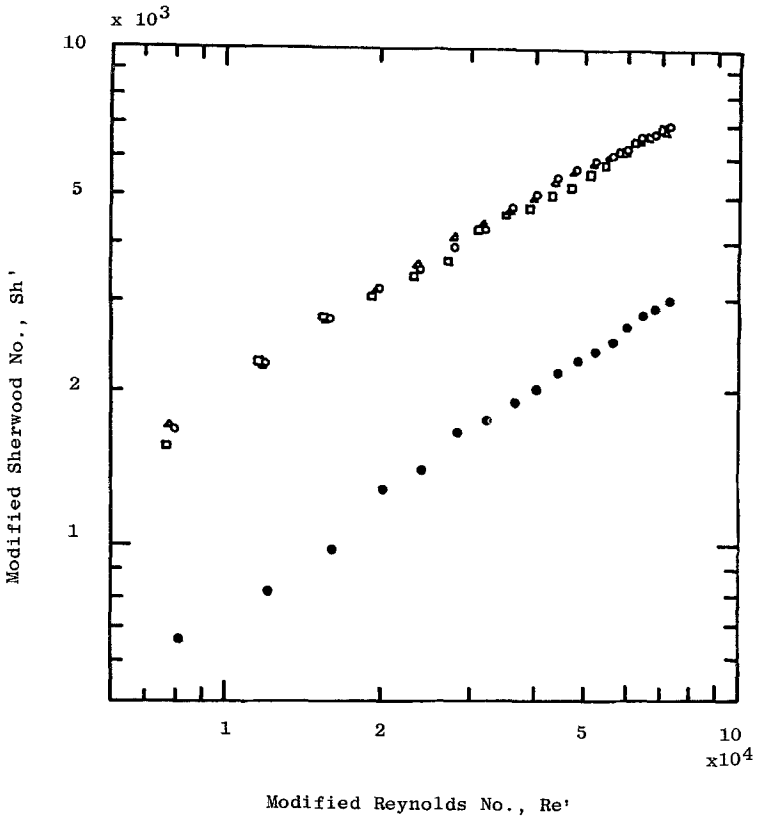

Fig. 5. Mass transfer correlations for longitudinally grooved cylinders PL1 to PL3 compared to smooth cylinder S3. ●, S3; ○, PL1; △, PL2; □, PL3.

4.1.2. Constant p/ε ratio; varying roughness height. The constancy of p/ε ratios for the same type of roughness elements implies geometric similarity. Electrodes PL1, PL2 and PL3, all with a p/ε ratio of 2.0, could be classified in this way. It is evident from Fig. 5 that, despite the variation in roughness height, the modified plot indicates an apparent similarity in performance. On average they produced an enhancement factor of between 2.6 and 2.4; the reduction in EF is attributable to a Reynolds number dependency in the region of 0.6 compared with 0.7 for a smooth RCE, i.e. a diminishing marginal enhancement with increase in Reynolds number. From Table 1, the *n*-exponents obtained using a least-squares method in the stated Reynolds number ranges refer to the mass transfer correlation expression of Equation 7. The notion of a wake-interference effect between adjacent regions would seem justified in the light of the variation in EF between these electrodes. For all three electrodes, crest width was virtually zero while roughness pitch varied between 0.635 and 1.45 mm. A further comparison between the modified performances of electrodes PL1, TL3 and TL5, all with comparable groove depths, gives greater credence to the above supposition concerning surface flow. Electrode PL1, which had perfectly formed 'V'-shaped roughness elements, was easily the most effective promoter amongst this latter group of electrodes.

4.2. *Circumferentially grooved cylinders*

From a hydrodynamic viewpoint this was probably the least complex roughness type investigated. This observation is supported through a comparison of the three curves in Fig. 6 in relation to the plot representing the performance of smooth electrode S3. To a degree, the rough electrode curves are almost parallel to the latter. It is seen that the correlation exponents, *n*, for electrodes PC1 and PC2, 0.688 and 0.179 respectively, are comparable to the 0.702 obtained for electrode S3. Presumably, the radial rechannelling of the interface flow within the surface

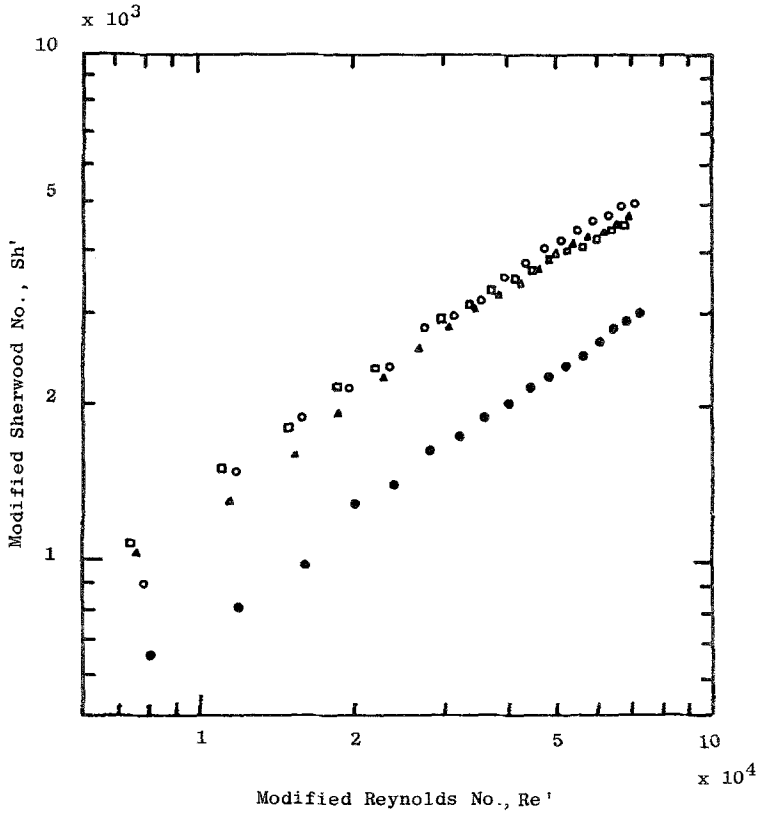

Fig. 6. Mass transfer correlations for circumferentially grooved cylinders PC1 to PC3 compared to smooth cylinder S3. ●, S3; ○, PC1; △, PC2; □, PC3.

troughs had little effect on the basic flow pattern. In other words, very little eddying occurred at this boundary. It may be expected that the greatest shearing action would be in the vicinity of the triangular crests where the lower resistance to diffusion would coincide with the local peak transfer coefficient values at the electrode surface. This effect must have accounted for a large proportion of the average 70% enhancement in transfer rate exhibited by the three electrodes.

The modified plot shows that for $Re > 15000$, mass transfer performance was independent of roughness height. However, electrode PC3, which represented the largest roughness pitch, seemed to undergo a marginal decline in performance for $Re > 40000$. For this reason, the curve representing electrode PC3 in Fig. 6 may be better correlated in two parts. A possible explanation for this drop in effectiveness at high Reynolds numbers may relate to the size of the pitch. Merely the girth of the groove may have resulted in a lower level of turbulence intensity within the grooves compared, for example with the situation at the surface of electrode PC1 where more sustainable eddying might have been achieved.

4.3. *Spirally grooved cylinders*

The roughness characteristics of electrodes PS1 to PS3 were similar to those described for the other two sets of grooved electrodes except that the roughness elements were machined 60° to the horizontal. The n-exponent varied from 0.541 to 0.587 thus indicating a lower Reynolds number dependency with increase in Reynolds number. When compared with electrodes PC1 to PC3, the intensity of eddy action within the grooves was bound to be more pronounced due to the groove inclination with regard to flow direction than was the case for circumferentially grooved electrodes. The combination of the above effect with the local peaks in current density expected at roughness crests ensured that the rate improvement at these surfaces was considerably higher.

Electrode PS2 ($\varepsilon = 0.50$ mm) performed in excess of PS1, but there was little difference

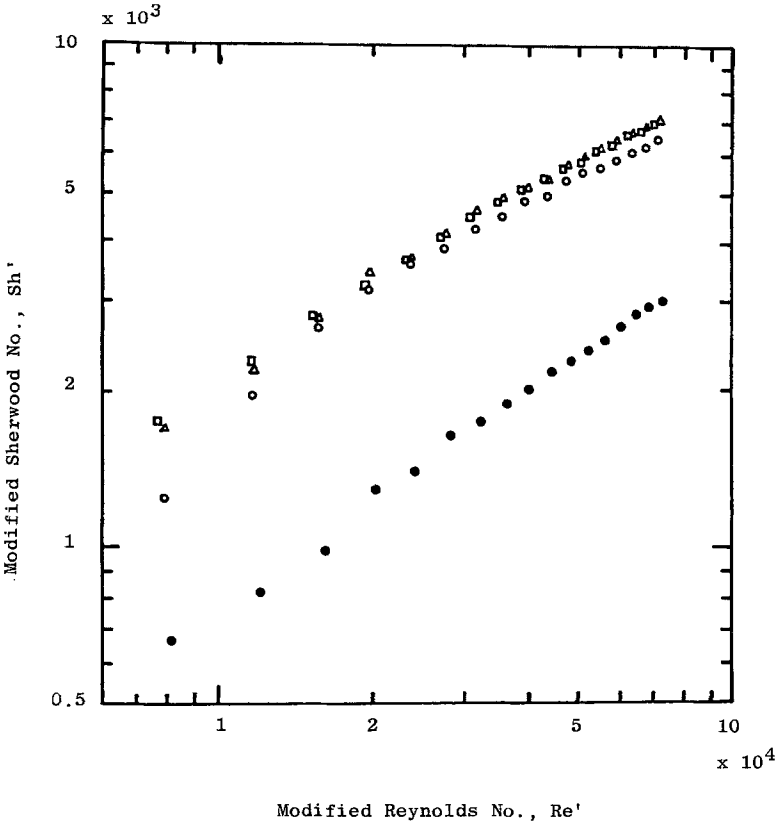

Fig. 7. Mass transfer correlations for spirally grooved cylinders PS1 to PS3 compared to smooth cylinder S3. ●, 3; ○, PS1; △, PS2; □, PS3.

between the former and electrode PS3. For $17\,000 < Re < 72\,000$ (Fig. 7) the mass transfer enhancement shown by PS2 varied from approximately 190 to 140%. Hence, more than double the rate improvement at PC-electrodes was achieved mainly due to hydrodynamic roughness effects in the form of higher shear.

A comparison between electrodes PL1 to PL3 and PS1 to PS3 indicates almost a duplication in terms of relative performances. Considering the fact that a typical spiral groove was inclined 60° to the horizontal, the similarity between the two sets of results and the distinct departure from circumferentially grooved electrode results does not overstate the significance of the orientation of a two-dimensional roughness element to fluid flow direction.

4.4. *Pyramid-knurled cylinders*

4.4.1. Effect of roughness height; constant pitch. Firstly, the pyramid-type roughness elements were more numerous than grooved elements. Furthermore, the three-dimensional characteristic provided a different form of interstitial flow pattern across the electrode surface. It is thus important to compare the results obtained with a truncated pyramidal element, representing each of the three roughness pitches, with the data which resulted from its perfectly formed opposite.

Electrodes TP1, TP2 and TP3 were knurled to give p/ε ratios of 2.75, 3.01 and 2.91, respectively. These figures compared with a ratio of 2.77 for the truncated, longitudinally grooved electrode, TL4. The p/ε value for electrodes PP1, PP2 and PP3 was the same, i.e. 2.0. Turning to Fig. 8 it is obvious that the performance of electrode TP3 was in no way less effective than that of PP3. In fact, above a value of $Re \sim 30\,000$, TP3 surpassed the latter in terms of mass transfer enhancement by an average 6%. This was in contrast to the 15% margin which separated the performances of electrodes PL3 and TL4 (both coarse pitched), the former having the advantage. On comparing the data

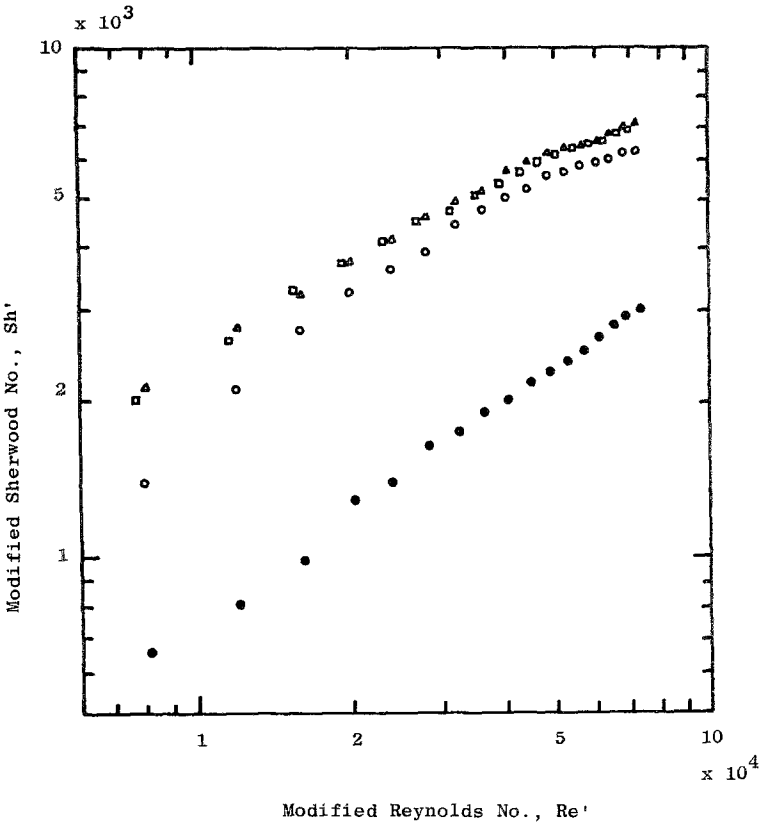

Fig. 8. Mass transfer correlations for pyramid-knurled cylinders TP1 to TP3 compared to smooth cylinder S3. ●, S3; ○ TP1; △, TP2; □, TP3.

obtained with electrodes TP2 and PP2 a similar deduction to that noted above applied, with the electrode that projected truncated elements providing about 3.5% marginal improvement. Again, the converse was true between electrodes PL2 and TL6. Such improvements are believed to be significant.

An interpretation of the above results has been based on possible flow patterns at electrode surfaces. As was mentioned earlier, flow eddies are probably 'captured' within triangular grooves at high Reynolds numbers. On the other hand, the flow stream would be expected to traverse paths of least resistance along the interstices, between and across pyramidal elements. Hence, the predominant type of surface promotion resulted from what have been described as 'horseshoe' eddies [18] which are generated between roughness elements and possibly around individual elements. As a consequence, whether truncated or not, the three-dimensional shape of these elements ensured that these 'horseshoe' eddies always exist with the same level of intensity at comparable Reynolds numbers.

Just beyond $Re = 12\,000$, electrodes TP1 and PP1 showed a distinct transition in performance level which was not in evidence for the other two pairs of electrodes. The initial steep increase in transfer coefficient prior to this transition stage may have been caused by what could be described as a 'smaller' eddying action at the surfaces of TP1 and PP1. Due to the relatively small roughness heights (0.0231 and 0.03175 cm), turbulence intensity around the elements may have been weaker than it later became a higher velocities. On the whole the margin of variation in relative performances between pyramid-knurled electrodes above $Re = 12\,000$ was low enough to be considered as having been caused by analytical error and the assumptions made in the evaluation of effective surface area.

4.4.2. Constant p/ε ratio; varying roughness height. Three electrodes which fitted the above description have already been mentioned in the

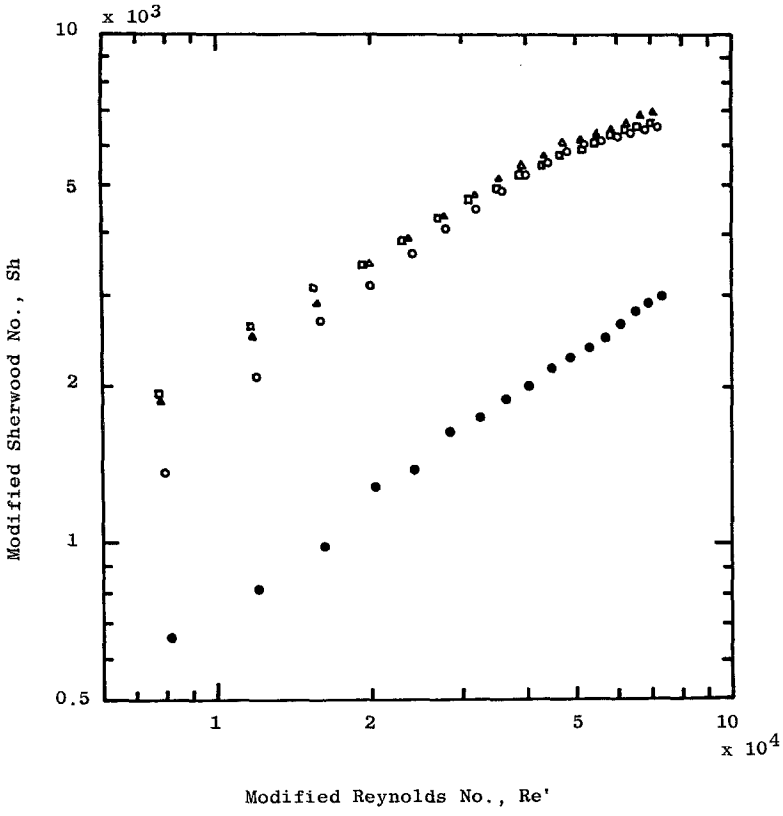

Fig. 9. Mass transfer correlations for pyramid-knurled cylinders PP1 to PP3 compared to smooth cylinder S3. ●, S3; ○, PP1; △, PP2; □, PP3.

preceding subsection. They were designated as PP1, PP2 and PP3. Apart from the first phase of the curve representing electrode PP1 in Fig. 9, i.e. below $Re = 12\,000$, all three electrodes provided relatively steady increments in transfer coefficient up to about $Re = 40\,000$. Mass transfer enhancement, which was established in the higher velocity range, varied from above 200% to a minimum of approximately 170% for these three electrodes. However, above $Re = 40\,000$ a definite deterioration in effectiveness was noticeable which corresponded to a very rapid decline in enhancement factor with increase in Reynolds number.

4.5. *Wire-wound cylinders*

It was also important to compare results reported for longitudinally grooved electrodes and those obtained at longitudinally wound wire electrodes, WR1 to WR3. The former represented an integrated, serrated macroprofile compared with the finer and more discrete nature of wire elements.

A simple correlation, taking the form of Equation 7, was performed for all the electrodes investigated. For the finest wire ($d = 0.05$ mm) the n-exponent was close to unity ($n = 0.991$). In the case of the other wire sizes there was a perceptible shift in curve gradient at about $Re = 42\,000$ to a value closer to 0.8 (Fig. 10). This implied that the marginal increment in transfer coefficient continued to rise steadily as the Reynolds number was increased, at least in the range investigated. Indeed, the enhancement factor for WR1 increased from barely 1.10 at $Re = 8470$ to just over 2.0 at $Re = 76\,000$. This type of behaviour was explained by Sheriff and Gumley [19] as indicating the need for the wire element to penetrate both the laminar sublayer and the buffer region sufficiently, by extending into the turbulent core, in order to be fully effective as a promoter. Electrode WR3 ($d = 0.125$ mm) was the most effective, registering an

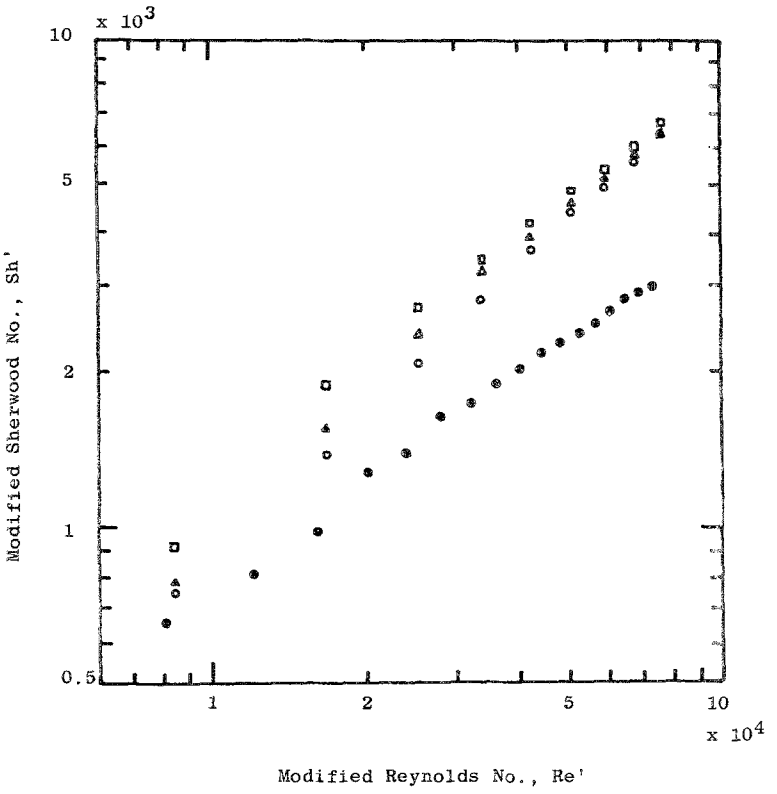

Fig. 10. Mass transfer correlations for wire-wound cylinders WR1 to WR3 compared to smooth cylinder S3. ●, S3; ○, WR1; △, WR2; □, WR3.

enhancement factor of about 2.20 at Re = 76 000.

On the basis of relative size and flow hydrodynamics, wire elements differ sharply from longitudinal grooves. For all its discreteness, a typical wire element produced an enhancement which belied its size; EF values approached those recorded with larger roughness elements at higher Reynolds numbers. Evidently, there exists a dissimilarity in the mechanism of turbulence promotion between a wire and a groove element. Storck and Hutin [20] inferred from their mass transfer distribution measurements across single and multiple wire elements that a maximum local transfer coefficient occurred just under each wire element. At higher speeds, a second and smaller peak appeared beyond the wire, this being attributed to a secondary wake-effect which extended some distance along the path between successive wire elements. This profile provides a good pictorial description of aspects of surface promotion which could not have been obtained from average mass transfer measurements.

4.6. *Weave-covered cylinders*

An example of a weave pattern is illustrated in Fig. 2. In order to give a definitive appraisal of surface promoters, it is customary to specify parameters such as roughness pitch and roughness height. However, the unusual structural form depicted in Fig. 2 does not satisfy these roughness definitions. Wire diameter expressed as 'ε' would ignore the double wire joints while width of opening, w, plus ε as roughness pitch would not account for the bulge where a shoot wire passes under a weft wire. The geometrical measurements are given in Table 1.

Mass transfer data from three weave-covered electrodes, WW1, WW2 and WW3, in order of increasing wire diameter, were reduced by dimensional analysis and a mass transfer correlation was attempted where linearity was detected from the curves shown in Fig. 11. Clearly, the curve representing electrode WW1 was anomalous in many respects when compared with the other two curves because at the lowest Reynolds number, WW1 was less effective than

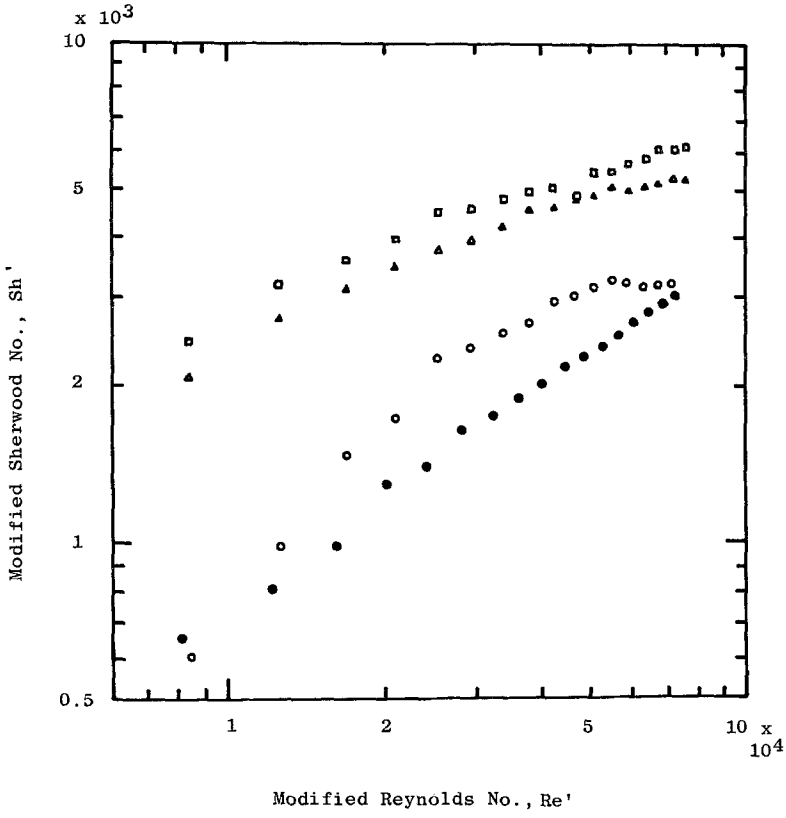

Fig. 11. Mass transfer correlations for weave-covered cylinders WW1 to WW3 compared to smooth cylinders S3. ●, S3; ○, WW1; △, WW2; □, WW3.

a smooth electrode. A similar performance pattern was also approached towards $Re = 76\,000$. In between these limits some enhancement was achieved up to about $Re = 25\,400$, following which marginal improvement declined sharply. At no point was the enhancement factor greater than 1.60. A possible explanation for this roughness behaviour relates to the relatively narrow constriction formed between wire elements at the surface of electrode WW1. At very low velocities the fluid probably skimmed over the weave surface, hence the low transfer coefficient measurements. As angular velocity was raised, the intensity of surface turbulence was increased thus leading to higher mass transfer coefficients.

The other electrodes in this group provided correlation patterns which were different to that described above. Although the wire sizes were in the ratio 1 : 1.30 : 1.77, the width opening, w, ratio was more diverse, namely 1.3 : 3.35 : 5.59. The relatively large size of the wire openings in the latter two cases would explain why such high enhancement factors were obtained at low Reynolds numbers. Unlike electrode WW1, hydrodynamic flow may not have been restricted in the manner described earlier; instead, local transfer rates were more pronounced. For electrode WW2 the first discernible linear region was for $12\,700 < Re < 38\,000$, with $n = 0.46$; the second, extending up to $Re = 76\,000$ gave $n = 0.22$. An almost identical pattern was shown by electrode WW3, although the first linear range covered only as far as $Re = 25\,400$. As was the case with electrode WW1, in the second half of the Reynolds number span, the enhancement factor dropped sharply. For instance, with WW2 the enhancement factor was above 3.0 at $Re = 15\,000$ but this had dropped to below 1.80 in the higher velocity range.

It will be recalled that a similar drop in performance occurred at approximately $Re = 40\,000$ for the entire group of pyramid-knurled electrodes. A common property shared by these electrodes and those used in the present study was the three-dimensional nature of their roughness characteristics, and it was probable that the

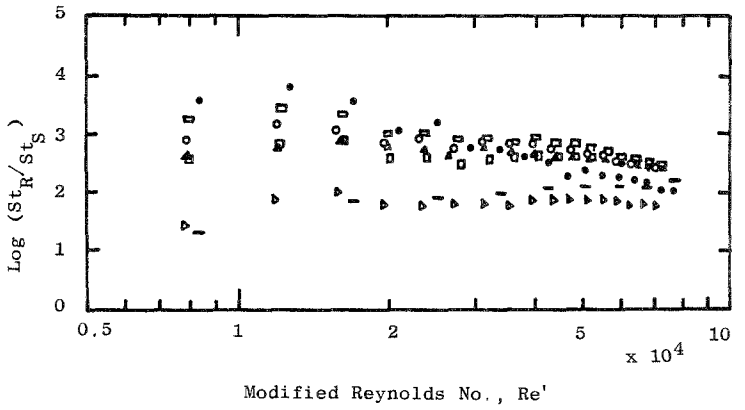

Fig. 12. Comparison of relative mass transfer performance for various types of roughness. ■, WR3; ▷, PC1; ●, WW3; □, TP2; ○, PP2; △, PL1; □, PS2.

level of turbulence intensity attained through eddying at low Reynolds numbers was not sustained as the angular velocity was increased. Through 'leakages', the surface eddies had short residence times within roughness crevices where they were most effective, and rapid fluid exchange with the bulk may have occurred because of adverse pressure differentials during rotation. This picture contrasts with the surface situation at spirally and longitudinally grooved electrode surfaces which were described earlier as perhaps becoming 'quasi-smooth' at higher velocities in conjunction with the concept of 'captured' eddies.

4.7. *Summary of roughness effects on mass transfer rates*

It was apparent that the quality of data analysis was improved through the introduction of roughness area factors, i.e. mass transfer enhancement less area enlargement contribution. As such, all the augmentation recorded accrued from the same source, namely surface promotion which represented the real measure of effectiveness. Implicit in the definition of enhancement factor, therefore, is its possible adoption as a directly comparable analytical quantity.

Seven electrodes, one each from the trio constituting every major type of roughness element investigated, are compared in Fig. 12. They were selected on the basis of being the most effective within their respective groups, but inevitably such a judgement was subjective in certain cases. Taken over the entire Reynolds number span there was sometimes only a marginal difference in performance between electrodes. The first conclusion which can be drawn from Fig. 12 is that effectiveness is selectively dependent on Reynolds number. It can also be deduced that three-dimensional elements were the best promoters, but only in the low Reynolds number ranges. These electrodes included PP2, TP2 and WW3, the wire-wound electrode WR3 providing the least improvement in this velocity range. While it must be borne in mind that neither WW3 nor WR3 could be judged with certainty to have represented optimum dimensions for mass transfer enhancement for their roughness types, it is nevertheless clear that whilst enhancement factor continued to decline for electrode PP2, TP2 and WW3 at higher Reynolds numbers, the opposite was observed with WR3. Hence, at sufficiently high velocities, electrode WR3 might produce an enhancement factor approaching 3.0 or even higher but less 'efficiently' than the other three electrodes.

Electrodes PL2, PS2 and PC1, on the other hand, gave significantly more consistent performances for $8000 < Re < 70\,000$. This was best evidenced by electrode PC1 with an enhancement factor averaging 1.80, i.e. an enhancement of 80%. However, this improvement was 80–100% below that produced by both PL2 and PS2, the latter two electrodes exhibiting almost identical enhancement capabilities. Hence, it is obvious that aligning two-dimensional roughness elements at an angle, θ, to the flow direction can provide improved mass transfer. However, the critical value of θ was not determined. From available

evidence, mass-transfer enhancement would be independent of θ for $30° < \theta < 90°$.

5. Conclusions

1. Artificial roughness elements located at an electrode surface can be expected to generate high levels of mass transfer enhancement in a turbulent regime. However, it is essential that the size of a roughness element be several order of magnitudes greater than the diffusion sublayer thickness.

2. Mass transfer enhancement was found to be independent of roughness height for geometrically similar roughness elements, i.e. those with similar roughness pitch to roughness height ratios, but its magnitude was a function of roughness type.

3. Roughness elements with three-dimensional character were superior to two-dimensional types, but only at the lower Reynolds number ranges. A maximum enhancement of 275% was recorded with a weave-covered RCE at $Re = 12\,700$.

4. With the exception of wire-wound electrodes, for which the Reynolds number exponent was consistently higher than 0.7 (as for a smooth RCE), the marginal increment in mass transfer coefficient for all other rough RCEs invariably declined at higher Reynolds number.

Reference

[1] A. E. Bergles, *Prog. Heat Mass Transfer* **1** (1969) 331.
[2] G. H. Sedahmed, A. Abdel Khalik, A. M. Abdallah and M. M. Farahot, *J. Appl. Electrochem.* **9** (1979) 563.
[3] R. Kappesser, I. Cornet and R. Greif, *J. Electrochem. Soc.* **118** (1971) 957.
[4] D. R. Gabe, *J. Appl. Electrochem.* **4** (1974) 91.
[5] D. R. Gabe and F. C. Walsh, *ibid.* **13** (1983) 3.
[6] F. S. Holland, *Chem. Ind. (London)* (1978) 453.
[7] D. R. Gabe and F. C. Walsh, *Surf. Technol.* **12** (1981) 25.
[8] F. C. Walsh, N. A. Gardner and D. R. Gabe, *J. Appl. Electrochem.* **12** (1982) 299.
[9] D. R. Gabe and F. C. Walsh, *ibid.* **14** (1984) 555, 565.
[10] *Idem, ibid.* **15** (1985) 807.
[11] P. A. Makanjuola and D. R. Gabe, *Surf. Technol.* **24** (1985) 29.
[12] P. A. Makanjuola, PhD Thesis, Loughborough University of Technology (1985).
[13] D. R. Gabe and P. A. Makanjuola, I. Chem. E. Symp. Ser. No. 96. (1986) p. 221.
[14] T. I. Quickendon and X. Jiang, *Electrochim. Acta* **29** (1984) 693.
[15] D. J. Robinson, PhD Thesis, University of Sheffield (1970).
[16] E. L. Jarrett and T. L. Sweeney, *AIChE. J.* **13** (1967) 797.
[17] J. T. Davies, Physiochemical Hydrodynamics Conference in honour of V. G. Levich (edited by B. Spalding), Adv. Publ., London (1977).
[18] P. R. Owen and W. R. Thompson, *I. Fluid Mech.* **15** (1963) 3.
[19] N. Sheriff and P. Gumley, *Int. J. Heat Mass Transfer* **9** (1966) 1297.
[20] A. Storck and D. Hutin, *Electrochim. Acta* **26** (1981) 127.